Chemistry–A European Journal
Full Paper
doi.org/10.1002/chem.202101988
Chemistry Europe
European Chemical Societies Publishing

Facile Synthesis of Platinum Right Bipyramids by Separating and Controlling the Nucleation Step in a Continuous Flow System

Ruhui Chen,[a] Yifeng Shi,[b] Minghao Xie,[a] and Younan Xia*[a, b, c]

Abstract: Colloidal synthesis of metal nanocrystals with controlled shapes and internal structures calls for a tight control over both the nucleation and growth processes. Here we report a method for the facile synthesis of Pt right bipyramids (RBPs) by separating nucleation from growth and controlling the nucleation step in a continuous flow reactor. Specifically, homogeneous nucleation was thermally triggered by introducing the reaction solution into a tubular flow reactor held at an elevated temperature to generate singly-twinned seeds. At a lower temperature, the singly-twinned seeds were protected from oxidative etching to allow their slow growth and evolution into RBPs while additional nucleation of undesired seeds could be largely suppressed to ensure RBPs as the main product. Further investigation indicated that the internal structure and growth pattern of the seeds were determined by the temperatures used for the nucleation and growth steps, respectively. The Br^- ions involved in the synthesis also played a critical role in the generation of RBPs by serving as a capping agent for the Pt {100} facets while regulating the reduction kinetics through coordination with the Pt(IV) ions.

Introduction

Synthesis of noble-metal nanocrystals with well-controlled sizes, shapes, and twin structures has been a major research focus in the field of nanomaterials over the past several decades because the properties and performances of nanocrystals in various applications critically depend on these parameters.[1] In particular, nanocrystals lined with twin defects, with notable examples including right bipyramids (RBPs),[2] decahedra,[3] and icosahedra,[4] have received extensive interest owing to their intriguing properties arising from the unique geometry and/or favorable strain fields associated with the twin defects.[5] Specifically, a RBP has six equivalent right-isosceles triangular side faces terminated in {100} facets, with a twin plane or a set of parallel planar defects through the equilateral triangle base, bisecting the particle into two halves in mirror image to each other.[2] In a previous study, Pd RBPs containing a single twin plane showed a specific activity 2.5 times greater than that of Pd cubes although both of their surfaces are enclosed by {100} facets.[2c] In other studies, it was reported that Cu and Ag RBPs exhibited fascinating optical properties due to their geometric anisotropy.[2a,d,e,g] These merits made nanoscale RBPs of noble metals interesting in both fundamental studies and practical applications.

Although progress has been made in the synthesis of nanoscale RBPs made of Pd, Ag, and Cu, only limited success has been achieved in the case of Pt.[2b] Due to its intriguing properties and catalytic activities, tremendous efforts have been devoted to the synthesis of Pt nanocrystals with desirable attributes in a rational and controllable manner.[6] Although the inclusion of twin defects provides an additional knob to engineer the surface properties of metal nanocrystals,[1d] it remains a challenge to synthesize Pt nanocrystals with twinned structures. This can be largely attributed to the high cost of energy associated with the formation of twin defects in Pt.[7] In a prior synthesis of Pt RBPs, this issue was addressed through the use of two specific Pt-binding peptides, BP7A and T7, to mediate the nucleation of singly-twinned seeds and direct the growth by stabilizing the Pt{100} facets, respectively.[2b] Despite the success in obtaining Pt RBPs, the products still need major improvements in terms of uniformity and purity before they can be employed to investigate and establish the structure-property relationship.

To obtain nanocrystals featuring a specific internal structure and shape, one needs to carefully manage both the nucleation and growth steps.[8] Previous studies have demonstrated that the internal structure of seeds produced during homogeneous nucleation is closely related to the initial reduction rate of a synthesis.[9] In particular, moderate initial reduction rates favor the generation of seeds with twinned structures, while fast and slow reduction kinetics encourage the formation of single-crystal and stacking fault-lined seeds, respectively. As such, the

[a] R. Chen, M. Xie, Prof. Dr. Y. Xia
School of Chemistry and Biochemistry
Georgia Institute of Technology
Atlanta, Georgia 30332 (USA)
E-mail: younan.xia@bme.gatech.edu
[b] Y. Shi, Prof. Dr. Y. Xia
School of Chemical and Biomolecular Engineering
Georgia Institute of Technology
Atlanta, Georgia 30332 (USA)
[c] Prof. Dr. Y. Xia
The Wallace H. Coulter Department of Biomedical Engineering
Georgia Institute of Technology and Emory University
Atlanta, Georgia 30332 (USA)
Supporting information for this article is available on the WWW under https://doi.org/10.1002/chem.202101988

initial reduction rate must be carefully tuned into an appropriate range to obtain singly-twinned seeds for the formation of RBPs. In the growth step, the nanocrystals with twin defects are highly vulnerable to oxidative etching, posing additional difficulty in producing RBPs.[10] Taken together, the nucleation and growth steps should be prudently manipulated, and in particular, separately controlled, to achieve the optimal conditions for each step. Different from a conventional one-pot synthesis in which the nucleation and growth are entangled with each other, intentional separation of these two processes has allowed tighter control over the size and shape of the nanocrystals.[11] Specifically, nucleation should be managed to produce a specific type of seeds for their growth into nanocrystals with the desired shapes and internal structures, but this process is extremely sensitive to the experimental parameters. For a conventional colloidal synthesis involving a batch reactor (*e.g.*, a vial or a flask), the spatial inhomogeneity in terms of temperature and composition may degrade the uniformity of the seeds and thus the quality of the nanocrystals.[12] In a set of recent studies, a continuous flow reactor was demonstrated as a powerful tool to achieve a tight control over the nucleation process and therefore improvement in product uniformity and purity.[11b,d] Compared with a batch reactor, the small lateral dimensions of a tubular flow reactor promote quick heat and mass transfer in the reaction solution while the reduction kinetics could be conveniently controlled to produce seeds with the desired internal structures.[11d,13] The continuous flow reactor also offers other advantages, including the distance-to-time transformation and linear scalability for potential mass production of nanocrystals.[14]

Herein, we report a facile method for the preparation of Pt RBPs by separating the nucleation and growth of colloidal nanocrystals into two steps and controlling the nucleation in a continuous flow system. Specifically, by pumping the reaction solution through a tubular flow reactor held at an elevated temperature, homogeneous nucleation was thermally triggered for 330 s to generate singly-twinned seeds. Afterwards, the seeds were allowed to slowly grow at a lower temperature, in an effort to protect the singly-twinned seeds from oxidative etching for their evolution into RBPs while eliminating additional nucleation of unwanted seeds. It was found that the Br^- ions involved in the synthesis played vital roles in the formation of RBPs by serving as a capping agent to Pt{100} facets for directing the shape evolution of the nanocrystals and as a ligand to Pt(IV) ions for regulating the reduction kinetics. As for the paired temperatures corresponding to the nucleation and growth steps, they were found to determine the internal structure and growth pattern of the seeds, respectively.

Results and Discussion

Figure 1 shows a schematic of the experimental setup used to separate nucleation and growth into two steps for the facile synthesis of Pt RBPs. Specifically, a tubular flow reactor was used to control the nucleation step by immersing one segment of a polytetrafluoroethylene (PTFE) tube in an oil bath held at

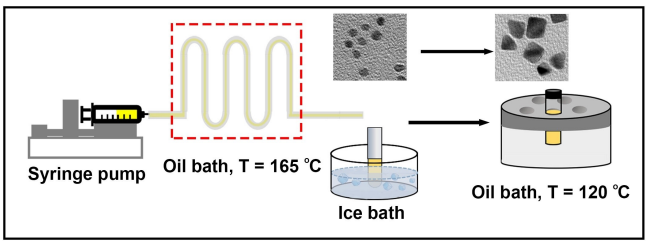

Figure 1. Schematic illustration of the experimental setup used for the preparation of Pt RBPs by separating growth from nucleation and controlling the nucleation step in a continuous flow reactor.

an elevated temperature. In a standard synthesis, the solution containing ethylene glycol (EG, a solvent and reductant), Na_2PtCl_6 (a precursor to Pt), KBr (a capping agent and coordination ligand), and poly(vinylpyrrolidone) (PVP, a colloidal stabilizer) was pumped into the tubular flow reactor at a flow rate of 0.1 mL/min. In this synthesis, EG served as both a solvent dissolving the chemicals and a temperature-dependent reductant reducing the Pt precursor to atoms for the nucleation and growth of Pt nanocrystals. The introduction of PVP as a colloidal stabilizer ensured the good dispersion of the nanocrystals in the solution while preventing their aggregation. When passing through the oil bath held at 165 °C, the precursor would be thermally triggered to reduce for 330 s, generating singly-twinned seeds through homogeneous nucleation. As reported in a previous study, the internal structure of the seeds formed in the early stage of a synthesis critically depends on the initial reduction rate.[9] As such, the reduction rate should be prudently tuned to a proper range in order to obtain seeds containing a single twin plane by adjusting the temperature for nucleation and the concentration of KBr. Detailed discussion will be presented at a later point. After flowing out of the reactor, the solution containing the just-formed seeds was collected by a test tube held in an ice bath to quench the reaction immediately and thus avoid additional nucleation events. In the presence of oxygen and halide ions, it is well documented that the singly-twinned seeds can be etched away by oxidative etching.[10] Therefore, the solution was transferred into a vial and then purged with argon to expel oxygen from the reaction system, in an effort to suppress oxidative etching and preserve the singly-twinned seeds during the growth stage. The tightly-capped vial was heated at 120 °C for 48 h, enabling slow growth of the seeds into RBPs.

Figure 2A shows typical transmission electron microscopy (TEM) images of the as-obtained Pt RBPs with a purity over 70%, as well as the models of individual RBP nanocrystals projected along four different orientations. The Pt RBPs had an average edge length of 7.0 ± 0.9 nm, which is defined by the leg length of the right isosceles triangular side faces. In addition to RBPs, nanocubes also appeared in the products as an impurity, likely owing to the fast reduction rate at the very beginning of the nucleation step for the generation of single-crystal seeds and subsequent formation of nanocubes. We conducted a control experiment by purging the reaction

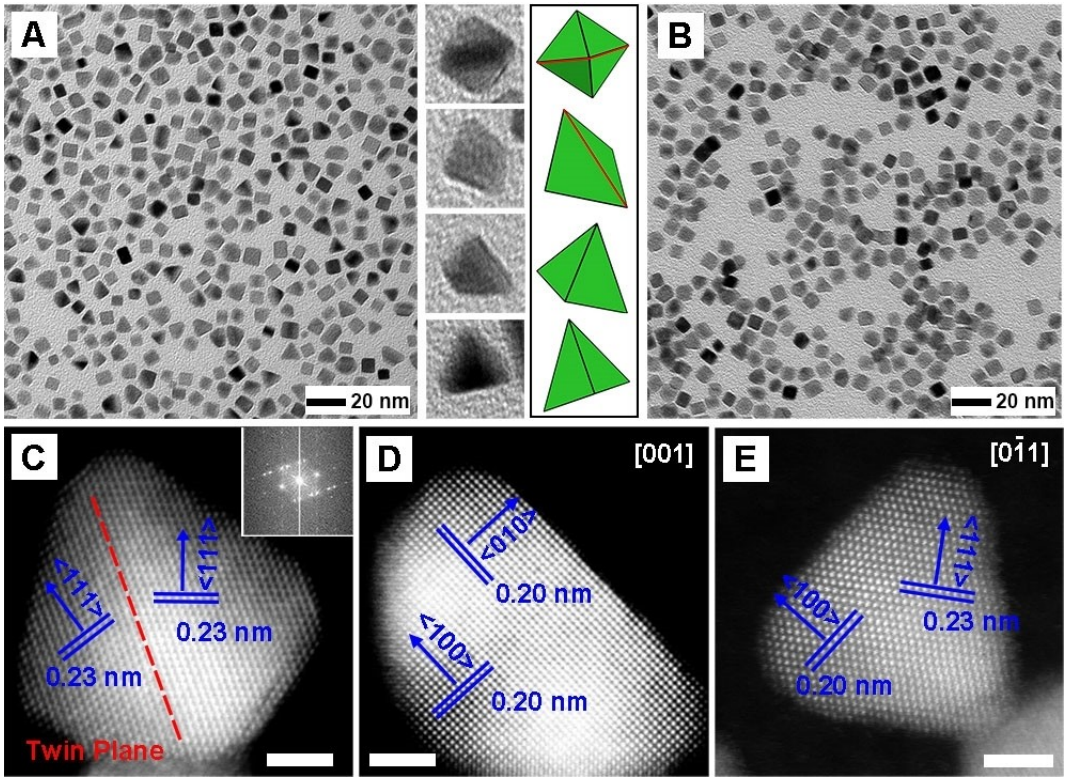

Figure 2. (A) TEM image of Pt RBPs synthesized by triggering nucleation at 165 °C for 330 s, followed by growth at 120 °C for 48 h. The models correspond to individual Pt RBPs in different orientations as shown by the magnified TEM images. The red line indicates the twin plane. (B) TEM image of Pt nanocrystals obtained by holding the reaction solution in a vial at 165 °C for 6 h, and the sample was dominated by single-crystal cubes rather than RBPs. (C) HAADF-STEM image of an individual Pt RBP with a single twin plane indicated by the red dashed line. The inset shows the corresponding Fourier transform pattern. (D, E) HAADF-STEM images of two Pt RBPs viewed along different directions. The scale bars in panels (C–E) are 2 nm.

solution held in a vial with argon and then allowing the reaction to proceed at 165 °C for 6 h. During this one-pot synthesis, homogeneous nucleation and growth were entangled with each other. In other words, multiple nucleation events also took place during the growth step, generating additional seeds throughout the synthesis. As shown in Figure 2B, the products were dominated by single-crystal nanocubes at a purity of 51 %, in addition to 27 % of RBPs and 22 % of rounded particles, validating that separation of nucleation from growth is critical to the formation of Pt RBPs. Similar to Pd and Ag RBPs,[2a,c] the Pt RBP contained a single twin plane with side faces covered by {100} facets, as revealed by close examination of the nanocrystals through scanning transmission electron microscopy (STEM). Figure 2C shows the high-angle annular dark-field (HAADF) STEM image of an individual Pt RBP, clearly demonstrating the presence of a twin plane bisecting the nanocrystal into two halves in mirror image to each other, as indicated by the red dashed line. Atomic-resolution images of slightly truncated Pt RBPs projected along two different directions are shown in Figure 2D and E. The results are in good agreement with a previous study of Ag RBPs, in that an odd number of twin planes resulted in the formation of RBP while even-numbered twin planes led to the generation of twinned cubes.[15] It should be pointed out that the pH of the reaction solution has significant impacts on the resultant nanocrystals. The introduction of additional H^+ or OH^- ions into the synthesis both led to the formation of polydispersed particles with a rounded profile while no RBPs were generated (Figure S1), which can be possibly ascribed to the involvement of etching in the reaction[16] and the variation in reduction kinetics.

The dominance of RBPs and nanocubes in the products shown in Figure 2A and B, respectively, is of particular interest and our further investigation revealed that this could be ascribed to oxidative etching involved in the synthesis, as well as the reduction kinetics. In the standard synthesis, homogeneous nucleation was thermally triggered in the flow reactor at 165 °C and the as-obtained seeds were then allowed to grow at 120 °C under the protection of argon. The lower temperature for the growth step greatly mitigated oxidative etching and thus the singly-twinned seeds were mostly preserved for their eventual growth into RBPs. In comparison, for the one-pot synthesis, although the vial was purged with argon prior to the reaction, it is difficult to completely remove the oxygen dissolved in the reaction solution. As such, at a high temperature of 165 °C, oxidative etching might still be able to take place at a relatively fast rate to etch away the singly-twinned seeds, removing RBPs from the final product while leaving behind single-crystal seeds for the formation of nanocubes. Therefore, a higher ratio of nanocubes relative to RBPs were obtained, while the co-existing rounded nanocrystals are likely

particles that have not fully developed to well-defined shapes as the precursor might be inadequate for the growth of the continuously generated seeds. To validate the proposed mechanism, another experiment was conducted by following the standard protocol except that the atmosphere in the growth stage was switched from argon to air. As shown in Figure S2, the resultant nanocrystals became a mixture of 58% of nanocubes and 42% of RBPs. In this case, the lower purity of RBPs than those obtained in the standard synthesis attested to the significance of inert atmosphere in protecting the singly-twinned seeds from oxidative etching. On the other hand, despite the presence of oxygen in the reaction system, the purity of Pt RBPs in this sample was still higher than that shown in Figure 2B, suggesting the suppression of oxidative etching at 120 °C and the importance of separating nucleation from growth in obtaining Pt RBPs as the main product.

Another plausible explanation for the dominance of nanocubes in Figure 2B lies in the fast reduction kinetics, as well as the occurrence of multiple nucleation events at 165 °C. A previous study has demonstrated that the precursor could be either directly reduced in the solution phase or adsorbed on the surface of a seed, followed by reduction to its atomic form, in the forms of solution and surface reduction, respectively.[17] In principle, the precursor should take the solution reduction pathway during homogeneous nucleation, while both surface and solution reduction could take place in the growth step. Specifically, an elevated temperature and fast reduction kinetics are usually required to enable solution reduction, while surface reduction is more favorable at a lower temperature under slow reduction kinetics because of its lower activation energy barrier than that of solution reduction.[17b] When the reaction solution was kept at a high temperature of 165 °C, solution reduction of the precursor would be enabled throughout the synthesis, and the continuous supply of Pt atoms allowed multiple nucleation events to occur. As a result of the fast reduction kinetics, single-crystal seeds were continuously formed, which then grew into nanocubes as the major product. As the reaction proceeded, the reduction rate would decrease due to the depletion of precursor, producing different types of seeds that finally evolved into RBPs and nanoparticles with rounded profiles. In the standard synthesis, the precursor took the solution reduction pathway to generate singly-twinned seeds at 165 °C, whereas surface reduction on the preformed seeds was more favored during the growth step at a lower temperature of 120 °C. As such, growth of Pt atoms was mainly confined to the surface of the singly-twinned seeds for their evolution into RBPs, while homogeneous nucleation of additional seeds in the solution phase was largely suppressed, ensuring RBPs as the major product of the synthesis.

It should be noted that, as confirmed by inductively-coupled plasma-mass spectroscopy (ICP-MS), only 20% of the precursor was consumed in the nucleation step and the large amount of precursor remaining in the solution could lead to additional nucleation events in the growth step. To figure out whether homogeneous nucleation occurred in the growth step, we performed a control experiment by holding the reaction solution containing 80% of the precursor used in a standard synthesis at 120 °C for 48 h while keeping all other parameters. As shown in Figure S3, in the absence of preformed seeds, homogeneous nucleation eventually occurred after a long period of time, and the as-obtained nanoparticles took a nearly spherical shape. However, almost no such particles were observed in the product prepared using the standard protocol, suggesting that homogenous nucleation was largely suppressed during the growth of the seeds. Moreover, with the continuous consumption of the Pt precursor as the reaction proceeded, the decelerated reduction kinetics would further diminish the possibility of the occurrence of homogeneous nucleation. These results attested that surface reduction prevailed during the growth stage, and the Pt RBPs were grown from the singly-twinned seeds formed during the nucleation step at 165 °C, instead of the possible seeds generated through self-nucleation at 120 °C. Since no additional, undesired seeds were formed during the growth process, Pt RBPs became the dominant species in the products shown in Figure 2A. Taken together, it can be concluded that the separation of nucleation from growth plays a critical role in obtaining Pt RBPs by preserving the singly-twinned seeds from oxidative etching while avoiding multiple nucleation events during the growth step.

In the present study, a continuous flow reactor was utilized to control the nucleation of the synthesis and thus obtain singly-twinned seeds. An immediate advantage offered by the flow reactor is that the reaction system is airtight during the nucleation process. In other words, the reaction solution had no contact with air and therefore the just-formed singly-twinned seeds could be well preserved, instead of being dissolved by oxidative etching. Additionally, compared with a batch reactor involving a large volume of solution, the small diameter of the tubular flow reactor (0.8 mm and 1.6 mm in inner and outer diameters, respectively) ensures quick heat transfer and thus faster equilibration between the temperature of the reaction solution and the surroundings (i.e., the oil bath).[11d,13] With a uniform spatial distribution of temperature in the flow stream, a tight control could be achieved over the reduction kinetics and thus the nucleation process. Besides, when quenching the reaction by cooling, the dropwise flow would allow quick equilibration of temperature with the ice bath, avoiding additional nucleation of undesired seeds. To support our argument, we conducted a control experiment by using a 20 mL glass vial of 23 mm in outer diameter to trigger the nucleation. Prior to the reaction, the vial was purged with argon to expel oxygen from the reaction system, in an effort to mitigate oxidative etching during the synthesis. Once the vial containing 5 mL of solution was put in the oil bath, the temperature of the oil bath immediately dropped from 165 to 160.5 °C and it was not brought back even at the end of the 330 s of nucleation. In contrast, when a tubular flow reactor was used to control nucleation, the temperature fluctuation of the oil bath was no greater than ±0.5 °C due to the slow introduction of reaction solution into the reactor, ensuring thermal homogeneity during the nucleation process. As shown in Figure S4, various types of Pt seeds with significantly different sizes were produced after the nucleation step, while the corresponding product obtained

after growth at 120 °C for 48 h only gave RBPs in low purity and poor size uniformity. This could be attributed to the uncontrolled reduction kinetics resulting from the slow heat transfer in a bulk amount of reaction solution. In this case, the temperature inhomogeneity during the nucleation process and formation of additional seeds when the solution was slowly cooled down in ice bath, both led to significantly degraded product quality. As such, the utilization of a continuous flow reactor is instrumental to a tight control over the nucleation of singly-twinned seeds for the formation of Pt RBPs. Moreover, taking advantage of the linear scalability of the flow reactor, it is feasible to scale up the synthesis for the potential mass production of Pt RBPs without compromising the product quality.

To elucidate the growth process of Pt RBPs, reaction intermediates were sampled at different time points during a standard synthesis and examined by TEM to track their shape evolution. After thermally triggering nucleation in the flow reactor at 165 °C for 330 s, seeds with a rounded shape and an average size of 3.1 nm were obtained (Figure 3A). Further characterization of the seed by STEM revealed that it contained a single twin plane, as marked by the red dashed line, attesting that Pt RBPs were grown from seeds featuring a singly-twinned structure. Under the protection of argon, the singly-twinned seeds then grew at 120 °C and evolved into slightly larger particles with a size of 4.5 nm after 6 h (Figure 3B). As we discussed previously, precursor reduction on the surface of the seeds is favored during growth due to the lower activation energy barrier to surface reduction than that to solution reduction, but the growth rate was relatively slow. When the duration of growth was further extended to 16 h, the nanocrystals were enlarged to an average size of 5.5 nm (Figure 3C), and around 50% of the nanocrystals grew into RBPs with truncated corners, in addition to 26% of nanocubes and 24% of rounded particles. At 24 h into the growth, 53% of the nanocrystals already developed into RBPs with an average size of 6.2 nm, while 18% and 29% of the nanocrystals were truncated RBPs and nanocubes, respectively (Figure 3D). The variation in the relative ratio of rounded particles, truncated RBPs, and RBPs in these intermediates indicated the evolution of singly-twinned seeds to RBPs with truncations and finally well-defined RBPs (Table S1). Collectively, singly-twinned seeds were formed during the nucleation stage at 165 °C, while the growth at a lower temperature was enabled by the reduction of precursor on the surface of the preformed seeds, generating RBPs as the final products.

In the present synthesis, Br^- ions were found to be critical in the formation of Pt RBPs as they not only served as a capping agent toward Pt{100} facets but also acted as a coordination ligand with the Pt(IV) ions to regulate the reduction kinetics. When different amounts of KBr were introduced into the standard synthesis, as shown in Figure 4, significant changes were observed for the shape and size of the as-obtained nanocrystals. In the absence of KBr during a synthesis, Pt nanoparticles with a nearly spherical shape were formed (Figure 4A), suggesting the vital role of Br^- ions in directing the

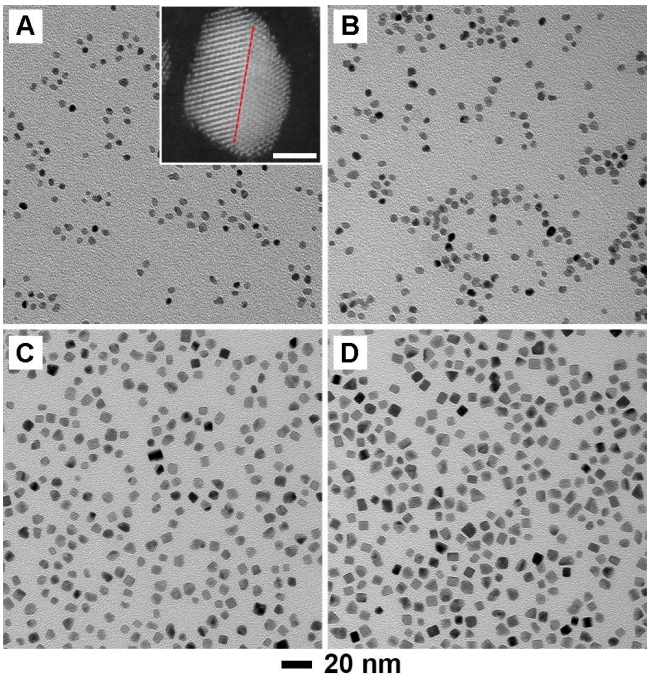

Figure 3. TEM images of Pt nanocrystals obtained in a standard synthesis after (A) nucleation at 165 °C for 330 s, and (B–D) nucleation at 165 °C for 330 s, followed by growth at 120 °C for (B) 6, (C) 16, and (D) 24 h, respectively. The scale bar at the bottom applies to all panels. The inset in panel (A) shows an HAADF-STEM image of an individual Pt seed containing a single twin plane, as indicated by the red dashed line (scale bar: 2 nm).

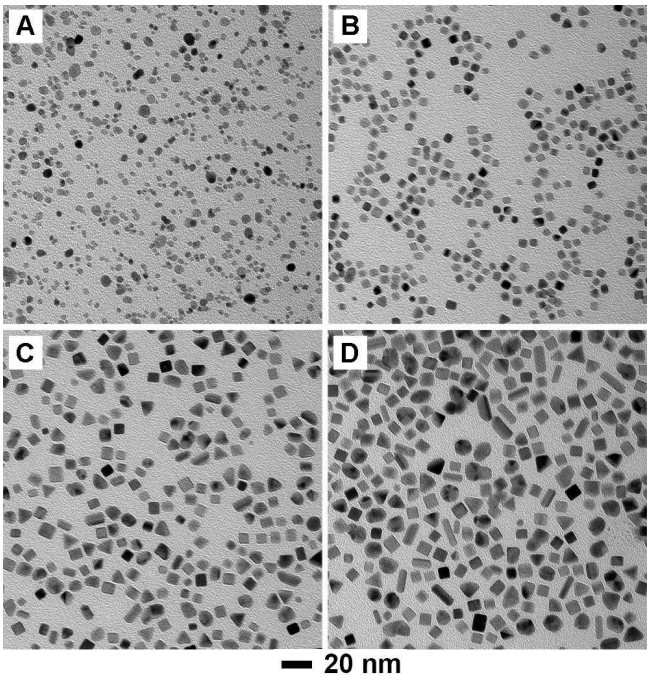

Figure 4. TEM images of Pt nanocrystals obtained using the standard protocol except for changing the concentration of KBr from 106 mM in the standard synthesis to (A) 0, (B) 35, (C) 159, and (D) 212 mM, respectively. With the increase of KBr concentration, the products changed from single-crystal to twinned structures and finally irregular particles, implying deceleration of the reduction kinetics.

shape evolution of Pt nanocrystals.[18] In contrast, when KBr was used at a concentration of 35 mM, the product became a mix of nanocubes, RBPs, and rounded particles at yields of 48, 26, and 26%, respectively (Figure 4B), attesting to the capping effect of Br^- to Pt{100} facets. It should be noted that, although the adsorption of Br^- hindered the deposition of atoms onto Pt {100} facets, those uncapped sites with higher surface energy, including the twin boundaries, edges and corners are still favored for atomic addition. Moreover, the surface of the nanocrystals is in dynamic changes throughout the synthesis because of the adsorption and desorption of Br^- and other surface species, allowing the deposited atoms to diffuse across the surface for the size enlargement and shape evolution of the nanocrystals. Additionally, it is well documented that Br^- can replace the Cl^- ions in the original precursor and coordinate to the metal center, generating $PtBr_6^{2-}$ as the actual precursor to Pt because of its higher stability constant relative to that of $PtCl_6^{2-}$.[19] As a result, the reduction kinetics could be slowed down owing to the more negative reduction potential of $PtBr_6^{2-}$. Compared with the standard synthesis involving KBr at 106 mM, the greatly reduced concentration of KBr enabled a faster reduction kinetics for the production of single-crystal seeds, while the capping effect from Br^- ions promoted the exposure of Pt{100} facets, generating nanocubes at a higher yield than that of RBPs. This is consistent with a previous study in that a slow initial reduction rate could trigger the formation of seeds with twin defects or stacking faults, whereas fast reduction kinetics favored the generation of single-crystal seeds.[9] In addition, rounded particles were produced at the same yield of RBPs, which can be attributed to the formation of a large quantity of seeds under fast reduction kinetics whereas the precursors were not adequate for all the particles to grow into well-defined shapes. With the further increase in KBr concentration to 159 and 212 mM, more nanoparticles with an irregular shape were observed in the products (Figure 4, C and D), in addition to nanocubes and RBPs. The occurrence of irregular particles can be attributed to the substantially slower reduction kinetics, generating seeds with different internal structures. Moreover, it is clearly observed that the size of the as-obtained nanocrystals became larger as the concentration of KBr was increased, suggesting that the reduction rate was slowed down and thus fewer seeds were formed in the nucleation step. Since the amount of precursor fed into the synthesis was fixed, more precursors would be allocated to each seed in the growth step, leading to an increase in size for the nanocrystals. Taken together, the use of KBr at a proper concentration is vital to the preparation of Pt RBPs, because of the dual roles of Br^- ions in capping Pt{100} facets and regulating the reduction kinetics. It is worth pointing out that the adsorption of Br^- ions on the surface could also affect the colloidal stability and growth pathway of the nanocrystals because the electrostatic repulsion between the negatively charged nanocrystals can prevent them from aggregation. In a prior study, it was demonstrated that the Pd nanoparticles with surface charge close to neutral could attach together to generate wavy nanowires, while the coverage of Cl^- ions on the seeds inhibited their attachment, allowing their growth to octahedra through atomic addition.[20] Therefore, in the present study, the Br^- ions may also contribute to the good dispersion of the Pt nanocrystals in the solution as well as to the evolution of the singly-twinned seeds to Pt RBPs through atomic deposition, instead of generating structures with other morphologies through particles attachment.

In addition to the concentration of KBr, the temperature used for triggering the nucleation should have a profound impact on the internal structures of the seeds and the resultant nanocrystals by affecting the initial reduction rate of a synthesis. To gain deeper insights into the formation of Pt RBPs, we conducted experiments by following the standard procedure while varying the temperature for the nucleation step. When the nucleation was allowed to proceed at a higher temperature of 175 °C, the purity of RBPs dropped to 59% and more nanocubes were observed in the products (Figure 5A). The lower purity of RBPs can be ascribed to the accelerated reduction kinetics at the elevated temperature, which resulted in the formation of single-crystals seeds and thus the generation of nanocubes. In comparison, lowering the temperature for nucleation to 155 °C led to a slower initial reduction rate. Consequently, less cubes were observed in the products, while multiply-twinned nanocrystals appeared, as indicated by the red arrows (Figure 5B). The main product became plate-like nanocrystals, which were actually RBPs with truncated corners, likely due to the overgrowth of RBPs in the presence of excess precursor. Owing to the slower reduction rate at 155 °C, less seeds could be produced during nucleation, and thus more precursors would be available to each seed for growth. After

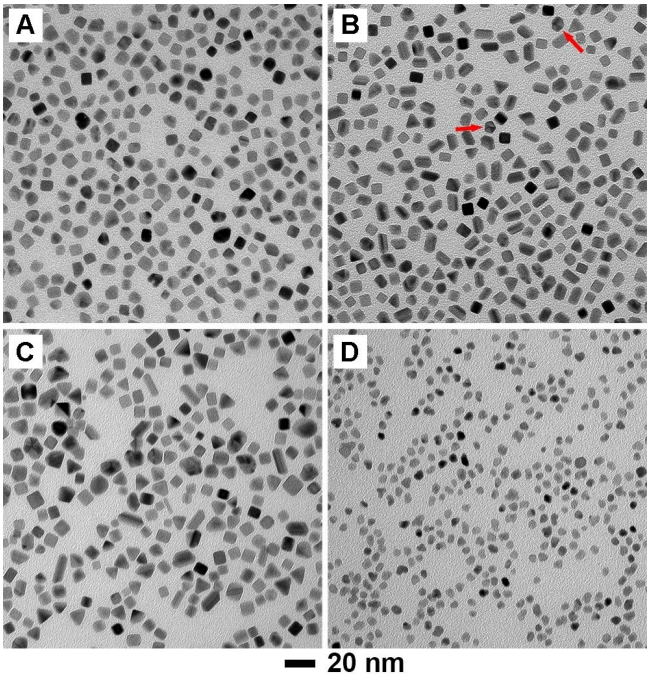

Figure 5. TEM images of Pt nanocrystals prepared by following the standard protocol except that the temperatures used for nucleation/growth were changed from 165/120 °C to (A) 175/120 °C, (B) 155/120 °C, (C) 165/140 °C, and (D) 165/100 °C, respectively. The red arrows indicate the multiply-twinned structures.

the seeds evolved into RBPs, the remaining precursor may lead to further deposition of atoms on the nanocrystals, which should selectively start from the twin defects because of the relatively high surface energy of these sites. However, the slow production of atoms by surface reduction as well as the sufficient adatom surface diffusion at 120 °C allowed the deposited atoms to migrate from twin defects to the edges and side faces of the nanocrystals, resulting in the formation of truncated RBPs. This is consistent with the result of a prior study, in which truncated Pd RBPs were generated through seeded growth from RBPs in the presence of additional precursor.[2c] Therefore, the temperature for triggering nucleation should be optimized in order to obtain a proper amount of singly-twinned seeds for the generation of RBPs. It is worth mentioning that the duration for the nucleation step also significantly influenced the product quality. As shown in Figure S5, both the decrease and increase in the nucleation time led to the degradation of product quality. A possible explanation for the observation is that the insufficient time for heating and triggering nucleation gave rise to seeds with poor quality while multiple rounds of nucleation took place over a long period of residence time, resulting in product polydisperse in both size and shape. Therefore, an appropriate duration for the nucleation step is important in obtaining high quality seeds for the formation of RBPs while ensuring the uniformity of the product.

Since the growth pattern of seeds also depends on the reduction kinetics, the influence of the temperature of the growth step on the resultant nanocrystals was investigated as well. As shown in Figure 5C, when the growth was carried out at an elevated temperature of 140 °C, a portion of the nanocrystals with smaller sizes was observed in the products, implying the occurrence of additional nucleation events during the growth step. At 140 °C, a temperature high enough to overcome the activation energy barrier for solution reduction, homogeneous nucleation was enabled, generating additional seeds and thus smaller nanocrystals due to their shorter duration of growth. Meanwhile, with the continuous consumption of the Pt precursor, the reduction rate was slowed down as the reaction proceeded. As such, irregular nanocrystals with unidentifiable internal defect structures, as indicated by the contrast observed in the TEM image of the particles, were generated as a result of the sluggish reduction kinetics. In a previous study on the synthesis of Pd nanoplates, particles taking such irregular shapes were also observed in the product when the reduction rate was very slow.[21] In comparison, at a low temperature of 100 °C, it was difficult to initiate growth on the seeds through surface reduction owing to the greatly decelerated reduction kinetics (Figure 5D). As a result of insufficient growth, the as-obtained nanocrystals exhibited a rounded shape and small sizes instead of evolving into Pt RBPs. Taken together, it is critical to choose a proper temperature to suppress homogeneous nucleation and formation of undesired seeds during growth while enabling reduction of the precursor on the surface of the seeds for their growth into RBPs. The size and yields of various nanocrystals under different experimental conditions were collectively summarized in Table 1, presenting the parameters vital in the formation of Pt RBPs.

Conclusions

In summary, we have developed a facile method for the preparation of Pt RBPs by separating the nucleation and growth of a synthesis into two steps. Particularly, a continuous flow reactor was utilized to control the nucleation step by thermally triggering the reduction of a precursor in the solution phase at a high temperature and thus enabling homogeneous nucleation to obtain singly-twinned seeds. The subsequent growth at a lower temperature preserved the singly-twinned seeds from oxidative etching for their slow evolution into RBPs while suppressing additional nucleation of unwanted seeds and thus ensuring RBPs as the major product. The Br^- ions introduced into the synthesis played vital roles in the formation of Pt RBPs by acting as a capping agent to promote the exposure of Pt {100} facets and a ligand to regulate the reduction kinetics through coordination to Pt(IV) ions. It was revealed that the pair of temperatures for the nucleation and growth steps had profound impacts on the formation of Pt RBPs by affecting the internal structure and growth pattern of the seeds, respectively. By separating nucleation from growth and controlling nucleation in a tubular flow reactor, each step could be conducted under optimal conditions for the generation of Pt RBPs. This work offers not only a facile route to the production of Pt RBPs but also a new approach that we could leverage for tightly controlling nucleation and growth for the synthesis of nanocrystals with desired shapes and structures.

Experimental Section

Chemicals and materials: Sodium hexachloroplatinate(IV) hexahydrate ($Na_2PtCl_6 \cdot 6H_2O$, 98%), potassium bromide (KBr, 99.0%), and poly(vinylpyrrolidone) (PVP, Mw ≈55,000) were all obtained from Sigma-Aldrich. Ethylene glycol (EG, ≥99.0%) was purchased from J. T. Baker. All chemicals were used as received. Deionized water with a resistivity of 18.2 MΩ cm at room temperature was used for the experiments.

Synthesis of Pt RBPs by controlling nucleation in a continuous flow reactor: In a standard protocol, 10 mg of $Na_2PtCl_6 \cdot 6H_2O$ were dissolved in 2 mL of EG under sonication. To verify whether sonication induced any reduction and nucleation in the solution, the precursor solution was centrifuged at 100,000 rpm for 1 h. No solid precipitate was observed and the concentration of the Pt(IV) ions remaining in the "supernatant" did not change before and after sonication, as confirmed by ICP-MS. Meanwhile, 3 mL of EG solution containing 50 mg of PVP and 63 mg of KBr were heated to 100 °C for 7 min to fully dissolve the chemicals, followed by natural cooling to room temperature. The two solutions were then mixed under magnetic stirring for 15 min to obtain a homogeneous reaction mixture. As shown in Figure 1, a PTFE tube with an inner diameter of 0.8 mm was utilized to trigger the nucleation process by immersing one segment of the tube in an oil bath held at 165 °C. Specifically, the reaction solution was continuously introduced into the preheated PTFE tube using a syringe pump at a flow rate of 0.1 mL·min^{-1} to initiate the reduction of the Pt(IV) precursor

Table 1. Summary of the size and yields of various nanocrystals under different experimental conditions.

Experimental conditions[a]	Size[b] [nm]	Yields of nanocrystals with different shapes
Standard protocol	7.0 ± 0.9	70% of RBPs, and 30% of nanocubes
Kept at 165 °C for 6 h	6.8 ± 1.3	51% of nanocubes, 27% of RBPs, and 22% of rounded particles
[KBr] = 0 mM	3.7 ± 1.9	All are nanoparticles with a nearly spherical shape
[KBr] = 35 mM	4.4 ± 0.7	48% of nanocubes, 26% of RBPs, and 26% of rounded particles
[KBr] = 159 mM	7.2 ± 1.5	61% of RBPs, 29% of nanocubes, and 10% of irregular particles
[KBr] = 212 mM	8.7 ± 2.2	42% of RBPs, 11% of truncated RBPs, 27% of nanocubes, and 20% of irregular particles
Nucleation at 175 °C	6.4 ± 1.2	59% of RBPs, 35% of nanocubes, and 6% of irregular particles
Nucleation at 155 °C	8.2 ± 2.2	19% of RBPs, 52% of truncated RBPs, 28% of nanocubes, and 1% of multi-twinned structures
Nucleation for 105 s	7.0 ± 1.2	5% of RBPs, 4% of nanocubes, and 91% of rounded particles
Nucleation for 450 s	6.5 ± 1.7	55% of RBPs, 7% of truncated RBPs, 26% of nanocubes, and 12% of irregular particles
Growth at 140 °C	8.3 ± 2.4	48% of RBPs, 32% of nanocubes, 10% of truncated RBPs, and 10% of irregular particles
Growth at 100 °C	4.2 ± 0.6	All are rounded particles
Growth in air	6.7 ± 1.3	42% of RBPs, and 58% of nanocubes
[HCl] = 24 mM	4.9 ± 1.6	2% of nanocubes and 98% of rounded particles
[NaOH] = 24 mM	Significantly varies from 1 nm to tens of nm	All are rounded and irregular particles

[a] For each control experiment, only the parameter listed in each row was changed while the other experimental conditions were kept the same as the standard protocol. [b] The size of nanocrystals refers to the leg length of the right isosceles triangular side faces of RBPs, the edge length of nanocubes, the height of the equilateral triangle base of truncated RBPs, or the diameter of the rounded particles.

and thus nucleation at the elevated temperature. Since the retention time of the solution in the flow reactor is determined by both the length of the segment being heated and the flow rate, the duration for nucleation could be controlled at 330 s by subjecting 204 cm of the tube to heating. After passing through the oil bath, the solution containing the just-formed seeds was collected by a test tube held in an ice bath to quickly quench the reaction and thus suppress the nucleation of additional, undesired seeds. The solution was then transferred into a 20 mL glass vial and bubbled with argon for 20 min to expel the oxygen from the vial and thereby suppress oxidative etching of the singly-twinned seeds during growth. Finally, the tightly capped vial was heated in an oil bath held at 120 °C for 48 h for the seeds to grow into Pt RBPs. After the synthesis, acetone was added into the reaction solution at a volume ratio of 7 to 3 and the mixture was centrifuged at 17,500 rpm for 15 min to collect the solid products. The as-obtained products were then washed twice with water and redispersed in water for further characterization.

Characterization: The TEM images were acquired on a Hitachi HT7700 microscope operated at 120 kV. The aqueous suspensions of the nanocrystals were drop-cast on carbon-coated copper grids and dried under ambient conditions prior to TEM analysis. The HAADF-STEM images were taken with a Hitachi HT2700 aberration-corrected STEM operated at 200 kV. To remove the remaining surfactants, the sample was washed 10 times with water and then treated in a Hitachi Zone cleaner for 30 min before imaging. Analysis of the metal content was performed with an ICP mass spectrometer (Perkin-Elmer, NexION 300Q).

Acknowledgements

This work was supported in part by a research grant from the NSF (CHE-1804970) and start-up funds from the Georgia Institute of Technology. Electron microscopy imaging was performed at the Georgia Tech Institute for Electronics and Nanotechnology, a member of the National Nanotechnology Coordinated Infrastructure (NNCI), which is supported by the National Science Foundation (ECCS-2025462).

Conflict of Interest

The authors declare no competing financial interest.

Keywords: continuous flow reactor · growth · nucleation · oxidative etching · right bipyramids

[1] a) E. C. Dreaden, A. M. Alkilany, X. Huang, C. J. Murphy, M. A. El-Sayed, *Chem. Soc. Rev.* **2012**, *41*, 2740–2779; b) M. Navlani-García, D. Salinas-Torres, K. Mori, Y. Kuwahara, H. Yamashita, *Catal. Surv. Asia* **2019**, *23*, 127–148; c) A. Zada, P. Muhammad, W. Ahmad, Z. Hussain, S. Ali, M. Khan, Q. Khan, M. Maqbool, *Adv. Funct. Mater.* **2020**, *30*, 1906744; d) Y. Shi, Z. Lyu, M. Zhao, R. Chen, Q. N. Nguyen, Y. Xia, *Chem. Rev.* **2021**, *121*, 649–735.
[2] a) B. J. Wiley, Y. Xiong, Z.-Y. Li, Y. Yin, Y. Xia, *Nano Lett.* **2006**, *6*, 765–768; b) L. Ruan, C.-Y. Chiu, Y. Li, Y. Huang, *Nano Lett.* **2011**, *11*, 3040–3046; c) X. Xia, S.-I. Choi, J. A. Herron, N. Lu, J. Scaranto, H.-C. Peng, J. Wang, M. Mavrikakis, M. J. Kim, Y. Xia, *J. Am. Chem. Soc.* **2013**, *135*, 15706–15709; d) Z. Lyu, M. Xie, K. D. Gilroy, Z. D. Hood, M. Zhao, S. Zhou, J. Liu, Y. Xia, *Chem. Mater.* **2018**, *30*, 6469–6477; e) E. Ringe, J. Zhang, M. R. Langille, C. A. Mirkin, L. D. Marks, R. P. Van Duyne, *Nanotechnology* **2012**, *23*, 444005; f) N. Lu, W. Chen, G. Fang, B. Chen, K. Yang, Y. Yang, Z. Wang, S. Huang, Y. Li, *Chem. Mater.* **2014**, *26*, 2453–2459; g) M. Tavakkoli Yaraki, S. Daqiqeh Rezaei, E. Middha, Y. N. Tan, *Part. Part. Syst. Charact.* **2020**, *37*, 2000027.
[3] S. Zhou, M. Zhao, T.-H. Yang, Y. Xia, *Mater. Today* **2019**, *22*, 108–131.
[4] H. Wang, S. Zhou, K. D. Gilroy, Z. Cai, Y. Xia, *Nano Today* **2017**, *15*, 121–144.
[5] J. L. Elechiguerra, J. Reyes-Gasga, M. J. Yacaman, *J. Mater. Chem.* **2006**, *16*, 3906–3919.
[6] a) Y.-J. Wang, W. Long, L. Wang, R. Yuan, A. Ignaszak, B. Fang, D. P. Wilkinson, *Energy Environ. Sci.* **2018**, *11*, 258–275; b) S. Sui, X. Wang, X. Zhou, Y. Su, S. Riffat, C.-j. Liu, *J. Mater. Chem. A* **2017**, *5*, 1808–1825; c) M. Miyake, K. Miyabayashi, *Catal. Surv. Asia* **2012**, *16*, 1–13; d) N. S. Porter, H. Wu, Z. Quan, J. Fang, *Acc. Chem. Res.* **2013**, *46*, 1867–1877.
[7] S. Kibey, J. B. Liu, D. D. Johnson, H. Sehitoglu, *Acta Mater.* **2007**, *55*, 6843–6851.
[8] a) Y. Xia, Y. Xiong, B. Lim, S. E. Skrabalak, *Angew. Chem. Int. Ed.* **2009**, *48*, 60–103; *Angew. Chem.* **2009**, *121*, 62–108; b) A. R. Tao, S. Habas, P. Yang, *Small* **2008**, *4*, 310–325.
[9] Y. Wang, H.-C. Peng, J. Liu, C. Z. Huang, Y. Xia, *Nano Lett.* **2015**, *15*, 1445–1450.
[10] a) R. Long, S. Zhou, B. J. Wiley, Y. Xiong, *Chem. Soc. Rev.* **2014**, *43*, 6288–6310; b) Y. Zheng, J. Zeng, A. Ruditskiy, M. Liu, Y. Xia, *Chem. Mater.* **2014**, *26*, 22–33.
[11] a) A. Janssen, Y. Shi, Y. Xia, *Chem. Eur. J.* **2020**, *26*, 13890–13895; b) J. Pan, A. O. El-Ballouli, L. Rollny, O. Voznyy, V. M. Burlakov, A. Goriely, E. H. Sargent, O. M. Bakr, *ACS Nano* **2013**, *7*, 10158–10166; c) K.-J. Kim, R. P. Oleksak, E. B. Hostetler, D. A. Peterson, P. Chandran, D. M. Schut, B. K. Paul, G. S. Herman, C.-H. Chang, *Cryst. Growth Des.* **2014**, *14*, 5349–5355; d) R. Chen, Z. Lyu, Y. Shi, Y. Xia, *Chem. Mater.* **2021**, *33*, 3791–3801.
[12] G. Niu, A. Ruditskiy, M. Vara, Y. Xia, *Chem. Soc. Rev.* **2015**, *44*, 5806–5820.
[13] E. Y. Erdem, J. C. Cheng, F. M. Doyle, A. P. Pisano, *Small* **2014**, *10*, 1076–1080.
[14] a) J. Sui, J. Yan, D. Liu, K. Wang, G. Luo, *Small* **2020**, *16*, 1902828; b) E. J. Roberts, L. R. Karadaghi, L. Wang, N. Malmstadt, R. L. Brutchey, *ACS Appl. Mater. Interfaces* **2019**, *11*, 27479–27502; c) P. Kunal, E. J. Roberts, C. T. Riche, K. Jarvis, N. Malmstadt, R. L. Brutchey, S. M. Humphrey, *Chem. Mater.* **2017**, *29*, 4341–4350; d) H. Song, J. D. Tice, R. F. Ismagilov, *Angew. Chem. Int. Ed.* **2003**, *42*, 768–772; *Angew. Chem.* **2003**, *115*, 792–796.
[15] M. McEachran, V. Kitaev, *Chem. Commun.* **2008**, 5737–5739.
[16] M. Liu, Y. Zheng, L. Zhang, L. Guo, Y. Xia, *J. Am. Chem. Soc.* **2013**, *135*, 11752–11755.
[17] a) M. A. Watzky, R. G. Finke, *J. Am. Chem. Soc.* **1997**, *119*, 10382–10400; b) T.-H. Yang, H.-C. Peng, S. Zhou, C.-T. Lee, S. Bao, Y.-H. Lee, J.-M. Wu, Y. Xia, *Nano Lett.* **2017**, *17*, 334–340; c) T.-H. Yang, S. Zhou, K. D. Gilroy, L. Figueroa-Cosme, Y.-H. Lee, J.-M. Wu, Y. Xia, *Proc. Natl. Acad. Sci. USA* **2017**, *114*, 13619.
[18] T.-H. Yang, Y. Shi, A. Janssen, Y. Xia, *Angew. Chem. Int. Ed.* **2020**, *59*, 15378–15401; *Angew. Chem.* **2020**, *132*, 15498–15523.
[19] a) X. Xia, Y. Wang, A. Ruditskiy, Y. Xia, *Adv. Mater.* **2013**, *25*, 6313–6333; b) H.-H. Li, S.-Y. Ma, Q.-Q. Fu, X.-J. Liu, L. Wu, S.-H. Yu, *J. Am. Chem. Soc.* **2015**, *137*, 7862–7868.
[20] Y. Wang, S.-I. Choi, X. Zhao, S. Xie, H.-C. Peng, M. Chi, C. Z. Huang, Y. Xia, *Adv. Funct. Mater.* **2014**, *24*, 131–139.
[21] L. Figueroa-Cosme, Z. D. Hood, K. D. Gilroy, Y. Xia, *J. Mater. Chem. C* **2018**, *6*, 4677–4682.

Manuscript received: June 7, 2021
Accepted manuscript online: July 27, 2021
Version of record online: August 31, 2021